Vietnam Journal of Earth Sciences, 43(4), 444-464, https://doi.org/10.15625/2615-9783/16444

Vietnam Academy of Science and Technology
Vietnam Journal of Earth Sciences
http://www.vjs.ac.vn/index.php/jse

Paleogene granite magmatism in the north of the Truong Son belt and implication for crustal evolution

Trinh Dinh Huan[1], Luu Cong Tri[1*], Nguyen Tuan Anh[2], Tran Viet Anh[2], Phan Hoang Giang[1], Nagi Takahashi[3], Boua Lay Saadsy[4]

[1]*General Department of Geology and Mineral of Vietnam, Hanoi, Vietnam*
[2]*Institute of Geological Sciences, VAST, Hanoi, Vietnam*
[3]*University of the Ryukyus, Okinawa, Japan*
[4]*Department of Geology and Mineral of Laos, Vientiane, Laos*

Received 14 June 2021; Received in revised form 01 August 2021; Accepted 15 October 2021

ABSTRACT

Abundant granitoids aged 24.59 Ma to 28.62 Ma were exposed along Phu Hoat high metamorphic zone, northern of the Truong Son belt, termed Na Khoun complex in Northern Laos (NL) and Ban Chieng complex in Western Vietnam (WV). Ten granitic samples were collected from these complexes show geochemical characteristics of high SiO_2 and K_2O contents, medium peraluminous that belong to S-type granites. Initial $^{87}Sr/^{86}Sr$ isotopic ratios and εNd(t) are broad values of 0.708507 to 0.74539 and -5.22 to -12.66, respectively, together with high $^{206}Pb/^{204}Pb$ (18.864-19.392), $^{207}Pb/^{204}Pb$ (15.736-15.841) and $^{208}Pb/^{204}Pb$ (39.224-40.080) which indicated crustal origin, we suggest that the NL-WV intrusion was associated with transpression form by the India-Asia collision events during Cenozoic.

Keywords: Truong Son belt, Cenozoic granites, Zircon U-Pb dating, Sr-Nd-Pb isotope.

1. Introduction

During the Cenozoic, the Southeast Asia region was bounded to the north and west by a Eurasian plate, to the south by the Indian-Australian plate (Katili, 1975; Hamilton, 1979). In 30 Ma ago, movement of the block driven by indentation of Eurasia by India plate (Tapponnier et al., 1982) continued further to the closure of the Proto-East Vietnam Sea (EVS), as Indochina was extruded South East on the sinistral Red River fault zone (Fig. 1a).

The Truong Son fold belt is located at the boundary between South China and Indochina blocks, also known as the Annamite Cordillera; this is an elongated mountain system composed of Paleozoic sedimentary and volcanic rocks (Hutchinson, 1993; Lepvrier et al., 1997; Zaw et al., 2014). The Truong Son fold belt is interpreted to have been developed from a Paleozoic volcano-

*Corresponding author, Email: luucongtri@gmail.com

sedimentary arc in the Paleo-Tethys Ocean (Fontaine and Workman, 1978; Hutchinson, 1993). The Phu Hoat high metamorphic zone in the northern Truong Son fold (Fig. 1b), consisting of a series of continuous overhanging blocks, is characterized by concentric metamorphic domes to which the metamorphic nuclear complex consists of sillimanite zones in the center and staurolite-disthene, almandine, biotite in the outer part. Magma activity in the Phu Hoat area occurs in many overlapping and complex phases (Fig. 2). It is widely accepted that the geochronological and geochemical data of granitic rocks can provide important information regarding the crustal evolution of tectonic plates. However, the geochronology and geochemistry of granitic rocks in Northern Laos are poorly known because there are few quantitative analysis results on geochemistry and isotopes. In recent years, we have collected more than 100 samples from different granitoid complexes in the Phu Hoat zone (Northern Laos and Western Vietnam) to reconstruct the convergence processes of Southeast Asian blocks during the closure of the Paleo-Tethyan Ocean. This paper presents new geochemical, geochronological data and isotopic characteristics of Northwestern Vietnam-Northeastern Laos magmatism.

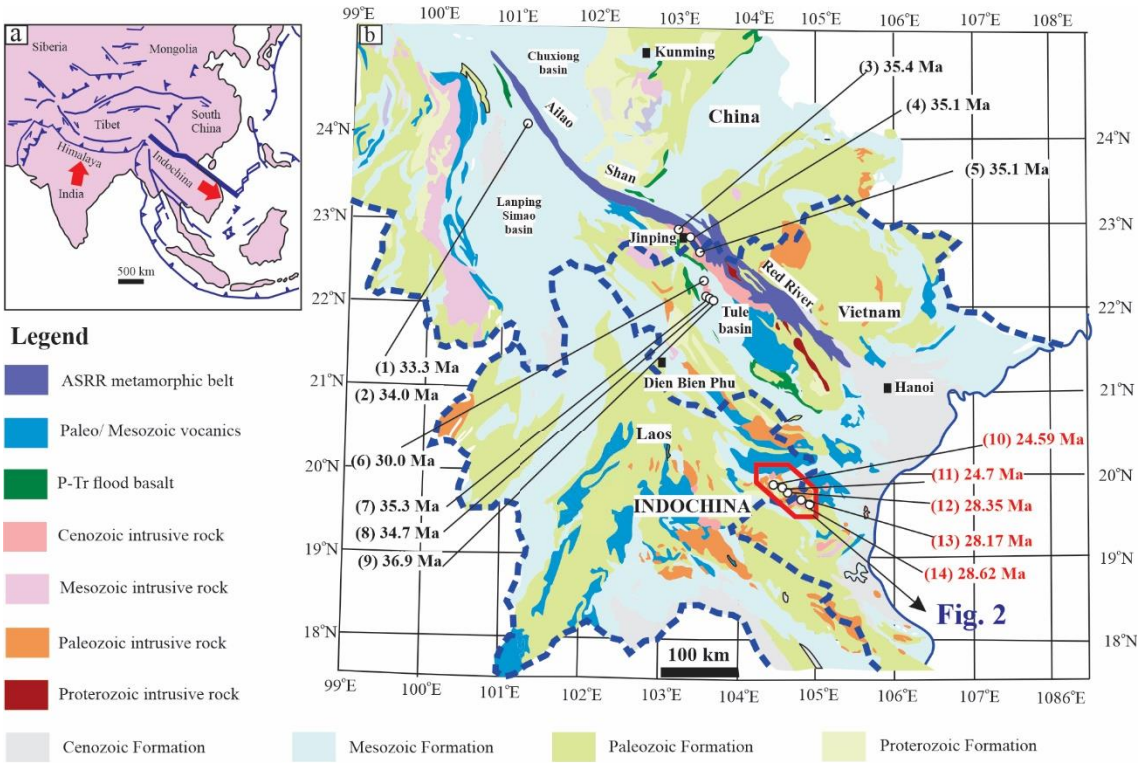

Figure 1. Simplified geological map in Eastern Ailaoshan-Red River.
a- The major Cenozoic fault systems in Asia (Schärer et al., 1990).
b- Geological map of the Eastern Ailaoshan Red River. Modifier from Lan et al. (2000)

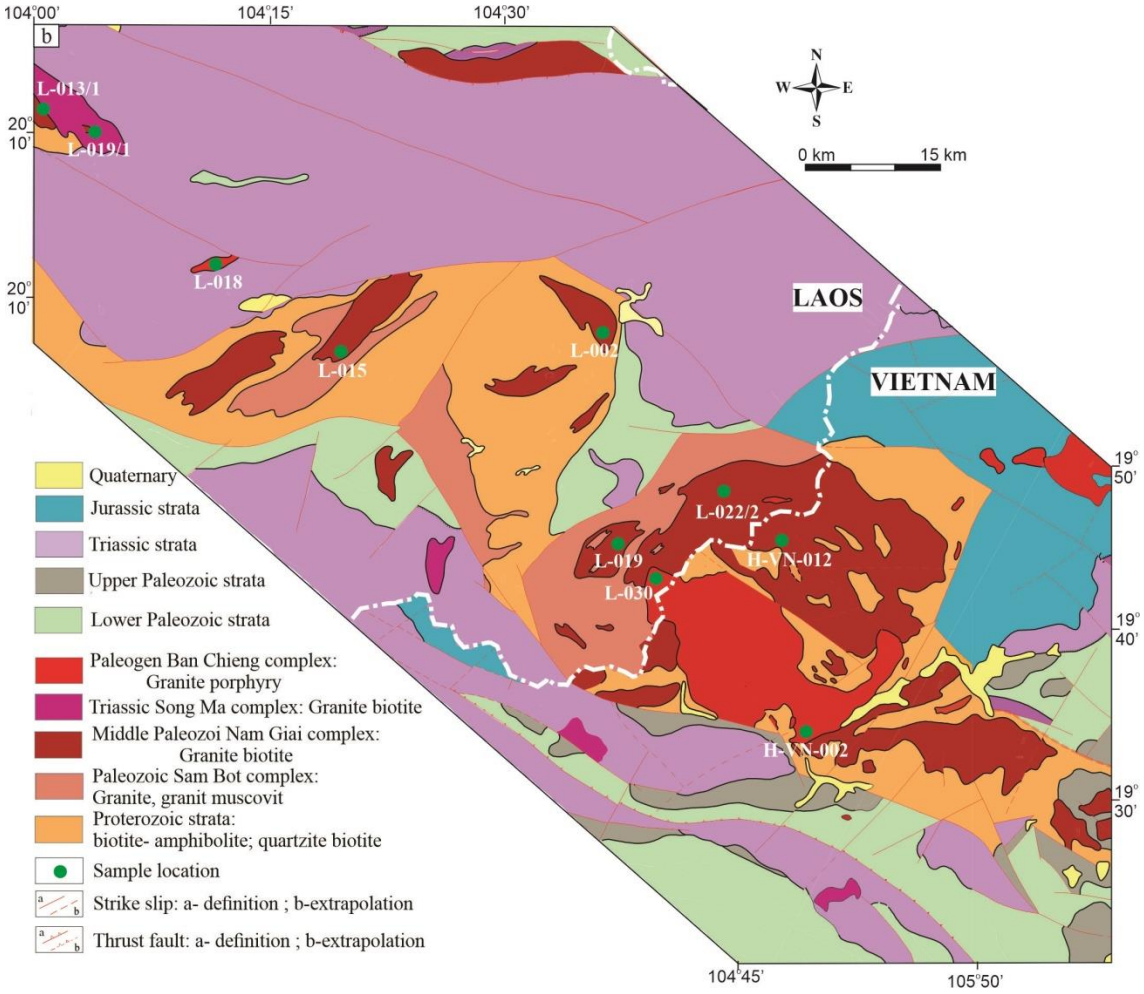

Figure 2. Geological map and sampling locations of Northern Laos and Western Vietnam (NL-WV)

2. Geological setting

The Truong Son belt is bounded by Song Ma shear zone in the North and Tam Ky-Phuoc Son in the South, extended for over 800 km in a northwest-southeast direction from North Central Vietnam through North Laos (Tran V.T. and Vu Khuc, 2011). It is composed of Precambrian-Cenozoic rocks. The Precambrian rocks are medium-high grade metamorphosed volcanic-sedimentary rocks that are locally exposed in the northwest, northeast, southeast, and south of the Truong Son belt. The Early Paleozoic (Middle Ordovician-Silurian) assemblages are characterized by a sequence of terrigenous flysch, cherty shale. Middle Paleozoic (Devonian-Early Carboniferous) sequence comprises Devonian-Lower Carboniferous terrigenous sediment in lower parts, grading upwards into limestone and cherty shale. The series rests unconformably upon older basalt conglomerates. The Upper Silurian-Lower Devonian sediments have conformable relation with the underlying sericitic shale. Carboniferous-Permian assemblages are highly differentiated, with the lower part consisting of coal-bearing terrigenous

sediments, grading upwards into shale, cherty-calcareous shale.

There are four main episodes of Paleozoic-Early Mesozoic magmatism that has been identified in the Truong Son belt: (1) Ordovician-Silurian (ca. 470-420 Ma): calc-alkaline volcanic rocks, granodiorite, and monzonite granite on the southwestern edge of the belt (Mao, 2012). These magmatic complexes are generally formed by subduction of the Tam Ky-Phuoc Son oceanic plate beneath the Truong Son belt. (2) Devonian-Early Carboniferous: magmatism of island arc type consists of diorite, biotite granite, and leucogranite (Kenzo et al., 2011). The rocks are volcanic arc granite related to the subduction setting. The volcanic rocks intruded into Middle Paleozoic sediment along the Truong Son belt and extended 260 km in the NW-SE direction. (3) Late Carboniferous-Early Permian (ca. 310-280 Ma): I-type granite, granodiorite, and diorite were emplaced in the southern Truong Son area (Ngo et al., 2014, 2016; Pham et al., 2017; Qian et al., 2020) were supported to be a subduction-related association with the Song Ma zone subduction lithospheric extension in response to north-dipping subduction of the Tam Ky-Phuoc Son oceanic plate. (4) Late Permian-Middle Triassic (ca. 270-245 Ma): S-type granites distributed in the Truong Son belt represent closure of the Song Ma suture zone, while synchronous I-type granite and volcanic rocks in the north represent south-dipping subduction of the Paleo-Tethys Song Ma oceanic plate beneath the Truong Son terrane (Pham N.C. et al., 2020; Wang et al., 2016; Tran et al., 2014). A small number of alkaline intrusions in the northern Truong Son terrane have Middle-Late Triassic ages (ca. 245-200 Ma) and were formed during the closure of the Song Ma ocean and collision of the South China and Indochina block.

3. Sample collecting and petrography

3.1. Samples collecting

Following the geological map of Laos and Vietnam, the samples were collected in Vietnam and Laos territories (Fig. 2). The main intrusive phase exposed on the field is composed of granosyenite, granite, and some granodiorite. These rocks penetrated Triassic volcano-terrigenous sediments, Neoproterozoic-Early Cambrian crystalline schist, and Late Paleozoic limestone (Figs. 1, 2).

3.2. Petrography

- Porphyry granite (L013, L018, L019, L030-2): medium to coarse grain size. Mineral composition (%): K-feldspar: 35-40, plagioclase: 15-25, quartz: 25-35, biotite: 3-5, rarely green hornblende (Fig. 3a, b).

- Granosyenite is porphyritic-textured (HVN002, L011): medium to coarse-grained size, pinkish-white K-feldspar in fined grain groundmass. The rocks are composed of K-feldspar on a medium-grained groundmass. Mineral composition (%): K-feldspar: 60-70, plagioclase: 5-10, quartz: 10-15; biotite: 2-7, rarely amphibole (Fig. 3e, f).

- Alaskite granite (HVN012, L002, L022): medium to fine-grained and xenomorphic texture. Mineral composition (%): K-feldspar: 60-65, quartz: 30-35; some plagioclase, chromatic minerals usually include biotite, rarely amphibole (Fig. 3c, d).

- Fine-grained leucogranite (L030-1): small vein formation transiting to aplite granite with granitic, aplitic, or granophyric texture. Its mineral composition is similar to that of porphyry granite.

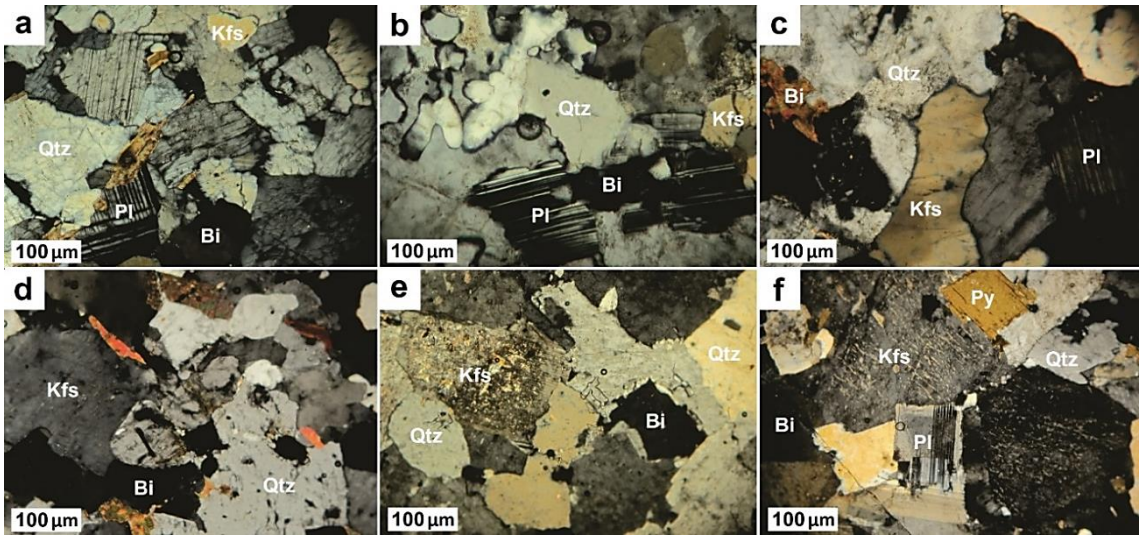

Figure 3. Photomicrographs showing microstructures and mineral components of granitoid rock in Northern Laos and Western Vietnam. *Qtz: Quartz; Ffs: K-feldspar; Pl: Plagioclase; Bi: Biotite*

4. Methodology

4.1. U-Pb zircon

Zircon crystals from five samples were separated from about 3-4 kg whole rocks after being crushed in a steel jaw crusher and shaking bed and heavy liquid and magnetic separation. Zircons were hand picking under a binocular microscope and set in an epoxy mount which was polished to expose zircons in half. The CL images were acquired with a SEM, JEOLJ SM-IT100A.

U-Pb zircon isotope analysis procedure was carried out at the Department of Physics and Earth Science, University of Ryukyus, Okinawa, Japan. Zircon U-Pb dating was performed using laser ablation inductively coupled plasma-mass spectrometry (LA-ICP-MS) Nu plasma II with a 193 nm excitation laser ArF system. The analysis points were selected in the growth fringe of zircon, where there is quite a clear zoning and no cracks. During the analysis, the zircon 91500 standard sample was analyzed simultaneously to check the stability of the analyzer and based on that, to correct the systematic errors. The analysis result of the standard zircon sample in this study is 1064±2.1 Ma, within the error range, completely similar to the $^{206}Pb/^{238}U$ age of 91500 zircon (1065.4±0.3 Ma) analyzed by Wiedenbeck et al. (1995). The zircon U-Pb isotope analysis results are processed by Isopot 3.0 software (Ludwig, 2003), and shown in Table 1, the analytical error is calculated as 1σ. More details on the analytical procedure can be found in Hisatoshi et al. (2017).

4.2. Major element composition analysis

About 25 g of chipped sample were crushed in a tungsten mill followed by grinding in a corundum mill. This portion is ready for major element (SiO_2, TiO_2, Al_2O_3, Fe_2O_3t, MnO, MgO, CaO, Na_2O, K_2O, and P_2O_5) analysis by XRF (X-Ray Fluorescence Analysis) on glass beads using a Bruker Pioneer at the University of Akita, Japan. The samples were randomly picked to re-analyze and evaluate analytical accuracy and precision at the Geological Survey of Japan using a PANalytical XRF analyzer.

The XRF analytical procedure is described as follows. The powdered samples were dried in an oven at about 100°C for about three hours then allowed to cool to eliminate surface water (humidity). Glass beads were made using 0.5 g of the dried powder mixed with 5 g of Li-tetraborate ($Li_2B_2O_7$) flux in a platinum crucible, heated to 115°C for the mixture to melt and homogenize totally. The Geological Survey of Japan and USGS standards (such as JB-1, JB-1a, JB-3, JA-1, JA-2, JR-1, JP-1, BHVO-2, and BCR-1) were used to construct the calibration lines and to verify the analytical accuracy and precision (Hoang and Uto, 2006). In general, the accuracy for the silicate oxides varies within ±1–2% (1σ). To estimate loss on ignition during the analysis, about 1.5 g of powdered sample were weighed in a clean 2 ml ceramic crucible and baked at about 1050°C for 3-5 h, sat to cool, then weighed.

4.3. Trace element analysis

About 50 mg of the baked sample was weighed in a 15 ml Teflon beaker for trace element composition analysis using an Agilent 8800 (Q)- ICP-MS at the University of Akita, Japan. The analytical procedure was described as follows. Samples were dissolved in mixtures of concentrated acid HNO_3 and HF by the ratio of 1:2 then left on a hotplate at 140°C for 48h. The samples are evaporated to complete dryness and then dissolved in 1 ml of 15N HNO_3, repeated twice to ensure that the sample was completely dissolved. The samples are then evaporated to dryness. About 6ml of 2N HNO_3 is added to form a dilution factor of about 63. The samples are left overnight on a hotplate at low temperature (ca. 80°C). About 0.2 ml of sample solution was weighed in ca. 15 ml of 0.3N HNO_3 to form a dilution factor of about 4600-4800 for analysis. A set of geological standards were analyzed whose results were used for the analytical calibration and data normalization. Based on repeated measurements of the geological standards, the accuracy of the trace elements varies between ±2–3% (1σ).

4.4. Sr-Nd-Pb isotope analysis

About 5 g of cleaned sample chips were ground in an agate mortar for the Sr-Nd-Pb isotopic analysis. A 50 mg portion is weighed and placed in a cleaned 15 ml Teflon beaker. Samples were dissolved in concentrated HNO_3-HF acids at 1:2 ratio on a hotplate at about 135-145°C for at least 48 h. The samples were evaporated completely, then dissolution in 2 ml of 2.5N HNO_3, ready for chromatographic work. Sr-spec was used to extract Sr and Pb, using diluted HNO_3 and strong HCl as eluants, respectively, to extract Sr and Pb. AG50W-X8-200 resin extracted rare earth elements, followed by Ln- resin to extract Nd (and Sm). The Sr, Nd, and Pb isotopic ratios were measured using a Neptune Plus MC-ICP-MS at the Department of Physics and Earth Sciences, University of the Ryukyu, Okinawa, Japan. During the isotopic analysis, $^{87}Sr/^{86}Sr$ of NBS987, a strontium isotopic standard, yielded a value of 0.71025±0.00015 (2σ, n=65), $^{143}Nd/^{144}Nd$ of JNDi-1, a Japanese neodymium standard, showed a value of 0.512116 ± 0.00013 (2σ, n=55); $^{206}Pb/^{204}Pb$, $^{207}Pb/^{204}$ Pb and $^{208}Pb/^{204}Pb$ of NBS981, a lead isotope standard, showed values, respective, of 16.939±0.004, 15.496±0.0057, 36.712±0.0182 (2σ, n=55).

5. Results

5.1. Zircons U-Pb geochronology

The U-Pb analytic results are listed in Table 1. The data show that these granitic rocks formed in two main stages: Early Oligocene (~28 Ma, HVN002; HVN012 and L0302) and Late Oligocene (~24Ma, L019; L013-1).

Table 1. Location, GPS, lithology, analyzing lab and average age dating results for 05 samples in NL-WV

No.	Sample ID	Area	Latitude	Longitude	Rock type	Average age
1	HVN002	Western Vietnam	19°33'38"	104°49'23"	Granosyenite	28.17±0.52 Ma
2	HVN012	Western Vietnam	19°45'21"	104°47'44"	Biotite granite	28.62±0.89 Ma
3	L030-2	Northern Laos	19°45'40"	104°39'36"	Porphyry granite	28.35±0.28 Ma
4	L013-1	Northern Laos	20°14'01"	104°00'08"	Porphyry granite	24.59±0.42 Ma
5	L019	Northern Laos	20°09'30"	104°01'55"	Porphyry granite	24.70±0.18 Ma

Analyzed at the University of Ryukyus, Japan

Zircon from the samples HVN002, HVN012, and L030-2 show mostly euhedral to subhedral, colorless and prismatic with 100 to 250 µm of length, and the ratio of length to width takes up 1:1 to 2.5:1, showing oscillatory zoning. Twenty-four analyses from the sample HVN002 gives a weighted mean age $^{206}Pb/^{238}U$ of 28.17 ±0.52 Ma (MSWD = 0.23; Fig. 4) with Th/U ratios range from 0.22-0.92 (> 0.1), indicated the zircons are magmatic origin (Hoskin and Black, 2000). Seven analyses from the sample HVN012 gives a weighted mean age $^{206}Pb/^{238}U$ of 28.62 ±0.89 Ma (MSWD = 0.6; Fig. 4). Nineteen analyses from the sample L030-2 show a weighted mean age $^{206}Pb/^{238}U$ of 28.35±0.28 Ma (MSWD = 0.37; Fig. 4).

Sixteen analyses from the sample L013-1 gives a weighted mean age $^{206}Pb/^{238}U$ of 24.59±0.42 Ma (MSWD = 0.33; Fig. 4). Ten analyses from the sample L019 show a weighted mean age $^{206}Pb/^{238}U$ of 24.70±0.18 Ma (MSWD = 1.2; Fig. 4).

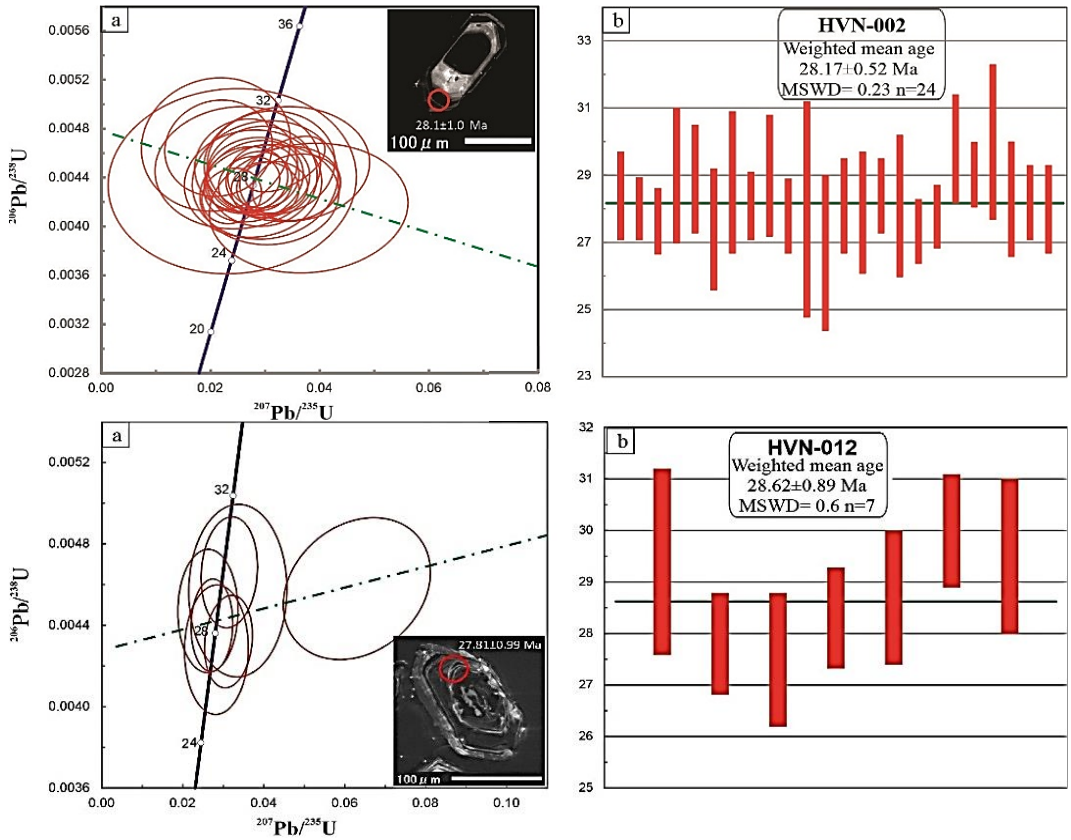

Figure 4. LA-ICP-MS zircon of five samples: a) U-Pb Concordia and CL images of zircon grains; b) Weighted mean ages

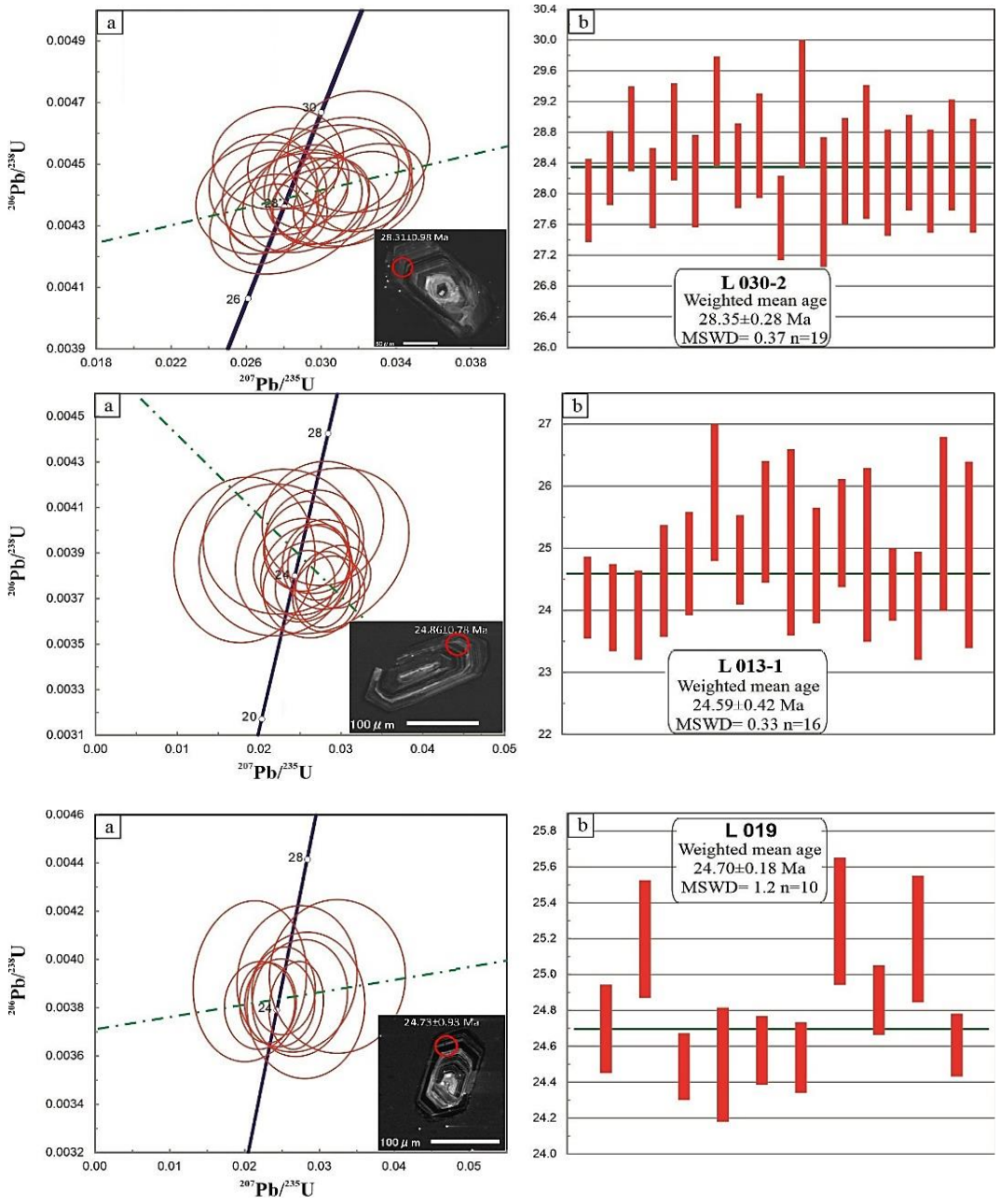

Figure 4. continue

5.2. Major and trace element composition

The whole-rock major and trace element compositions for NL-WV are given in Table 2. These rocks show high SiO_2 contents varying from 67.6 to 74.4 wt %, total alkaline (Na_2O+K_2O) range from 5.66 to 9.01%, corresponding granites field, and high K-calc alkaline series (Fig. 5a, c). The CIPW-normative mineral compositions from the bulk chemical analysis have 23-33 vol. % Qtz, 20-41 vol. % Or, 16-31 vol. % Ab, 2-13 vol. % An, and 0.00-2.41 vol. %

corundum (Fig. 5d). The calculation data for the Aluminum Saturation Index (ASI) of these granitic rocks range from 1.40 to 1.67. Most samples have relatively high A/CNK values, implying medium peraluminous (Fig. 5b, c). The zircon saturation temperatures (Watson and Harrison, 1983) were calculated from granitic compositions range 658°C to 847°C.

In the chondrite-normalized REE diagram, the granites are marked by significant enrichments in light REEs and depletions in heavy REEs, $(La/Yb)_N$ = 6.52-101.76 and negative Eu anomalies (Eu/Eu* = 0.35-0.88), suggesting significant plagioclase fractionation during magma evolution. A similar pattern of Northern Laos and Western Vietnam granite with Upper continental crust on the primitive mantle-normalized trace-element diagram with enrichment in Rb, Th, K, U, and Pb, depletion in Sr, Ba, Ce, Nb, Ti. (Fig. 6b).

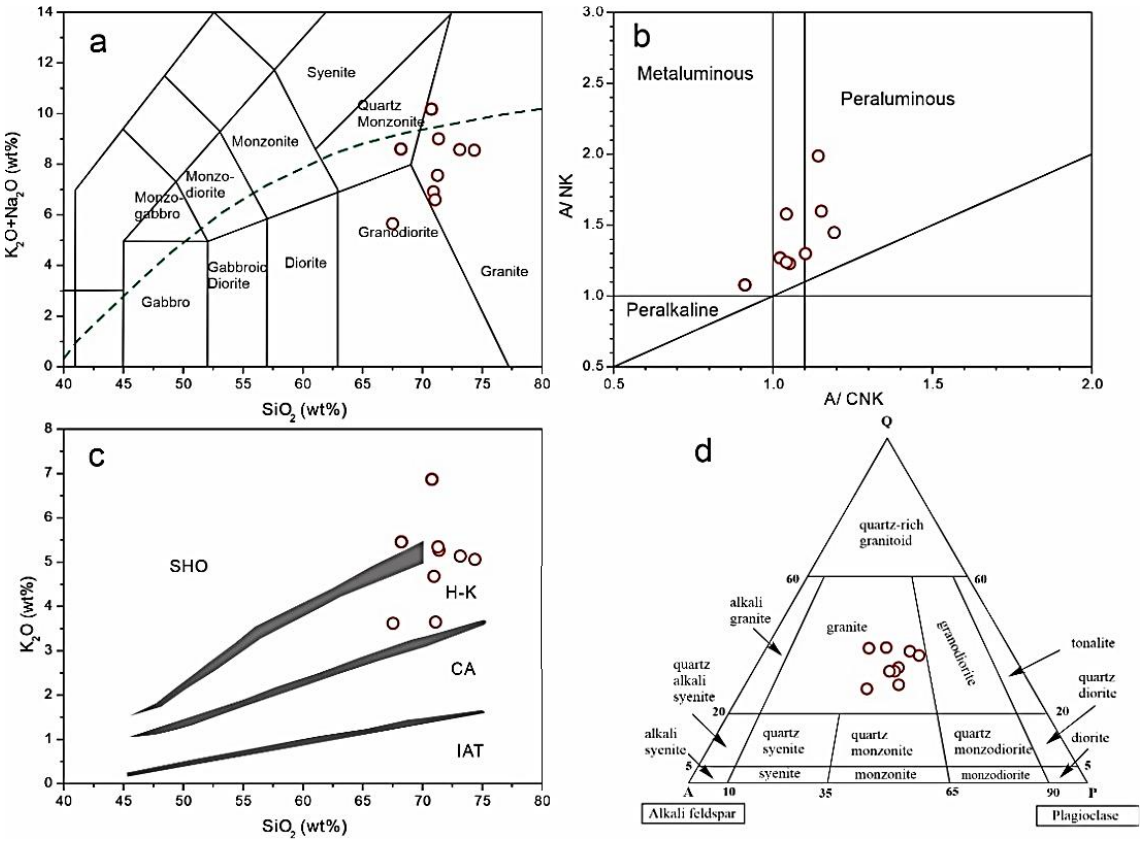

Figure 5. Major elements of Northern Laos-Western Vietnam granites: a) (K_2O+Na_2O) vs. SiO_2 (Middlemost, 1994); b) molar Al_2O_3/(Na_2O + K_2O) vs. molar Al_2O_3/(CaO+Na_2O+K_2O) (Maniar and Piccoli, 1989); c) SiO_2-K_2O diagram (Wood, 1989); d) QAP diagram

Table 2. The whole-rock major (wt%) and trace (ppm) element compositions for the granite from NL-WV

	HVN002	HVN012	L002	L011	L013/1	L018	L019	L022/2	L030
SiO_2	68.24	70.81	71.40	71.32	74.39	70.98	73.18	67.55	71.12
TiO_2	0.37	0.20	0.30	0.58	0.12	0.61	0.26	0.62	0.37
Al_2O_3	14.07	13.87	15.36	13.65	13.84	13.95	13.94	14.44	13.86
Fe_2O_{3t}	2.53	1.67	1.94	3.61	1.14	3.81	1.91	5.07	3.60
MnO	0.04	0.02	0.03	0.04	0.03	0.06	0.04	0.10	0.05
MgO	0.44	0.28	0.35	0.85	0.20	0.96	0.38	2.55	0.69
CaO	1.47	1.27	1.14	1.13	1.07	1.89	1.17	2.96	2.52
Na_2O	3.14	3.29	3.74	2.22	3.49	2.22	3.44	2.03	2.94
K_2O	5.46	4.65	5.27	5.35	5.07	4.69	5.14	3.63	3.66
P_2O_5	0.10	0.05	0.07	0.13	0.03	0.14	0.07	0.11	0.08
LOI	4.15	3.89	0.41	1.11	0.61	0.68	0.47	0.94	1.11
Total	100.00	100.00	100.00	100.00	100.00	100.00	100.00	100.00	100.00
Li	39.60	104.80	27.01	12.71	34.53	19.01	31.20	33.86	23.98
Be	3.98	6.35	4.03	2.72	7.58	2.61	5.46	2.17	2.20
Sc	4.57	3.35	4.25	8.63	4.53	9.30	5.42	14.95	12.30
V	17.74	9.23	16.54	42.17	10.76	42.68	18.62	90.92	37.82
Cr	2.10	2.84	5.36	22.07	4.11	23.94	6.12	67.73	9.04
Co	3.06	1.47	2.76	5.32	1.45	7.36	3.38	14.95	6.06
Ni	1.19	1.02	6.94	13.62	7.21	13.31	7.09	34.56	6.48
Rb	282.50	351.40	226.30	247.67	375.66	238.16	364.46	190.33	166.64
Sr	147.50	129.60	399.59	77.74	90.06	87.59	117.83	272.06	131.92
Y	33.01	26.97	15.58	41.75	45.78	43.59	47.21	29.42	41.81
Zr	32.36	80.20	209.55	277.66	99.75	260.56	170.87	161.94	222.85
Nb	23.38	38.02	24.04	12.61	25.64	12.90	20.52	11.29	10.80
Ba	581.10	650.90	859.87	831.40	315.78	755.63	466.96	560.90	890.73
Cs	10.50	13.71	3.16	7.38	8.41	5.05	11.49	11.95	7.93
La	87.04	58.95	78.15	41.85	27.91	42.90	36.17	20.28	46.40
Ce	169.00	114.10	156.50	83.15	56.05	86.22	73.81	38.91	115.80
Pr	16.50	11.52	12.59	9.44	6.41	9.77	8.26	4.49	10.32
Nd	52.83	37.73	38.27	33.56	22.36	35.53	29.31	16.77	37.80
Sm	8.28	6.75	5.30	6.86	4.83	7.30	6.27	3.55	7.60
Eu	1.20	0.76	1.09	1.11	0.63	1.23	0.74	1.07	1.38
Gd	7.55	6.46	5.30	6.99	4.79	7.43	6.34	3.89	7.88
Tb	0.97	0.87	0.52	1.06	0.76	1.11	0.99	0.63	1.19
Dy	5.28	4.53	2.15	6.16	4.83	6.32	6.04	3.86	7.04
Ho	1.02	0.81	0.36	1.23	0.95	1.24	1.26	0.81	1.42
Er	2.83	2.11	0.82	3.34	2.86	3.47	3.82	2.37	3.95
Tm	0.41	0.29	0.09	0.46	0.44	0.45	0.58	0.35	0.57
Yb	2.66	1.86	0.55	2.66	2.79	2.68	3.75	2.23	3.54
Lu	0.38	0.26	0.05	0.35	0.41	0.33	0.55	0.32	0.51
Hf	0.92	1.96	0.26	2.09	1.10	1.76	1.64	0.58	2.34
Ta	1.40	2.75	2.26	1.02	2.09	1.16	3.39	1.11	1.01
Pb	27.60	19.45	61.85	19.44	42.35	34.70	41.71	31.08	29.45
Th	32.92	40.54	50.10	19.01	27.31	18.94	33.62	9.46	13.88
U	10.22	7.85	6.61	4.87	13.42	5.53	14.29	2.59	4.28
A/CNK	1.40	1.51	1.51	1.57	1.44	1.58	1.43	1.67	1.52

Analyzed at the University of Akita, Japan

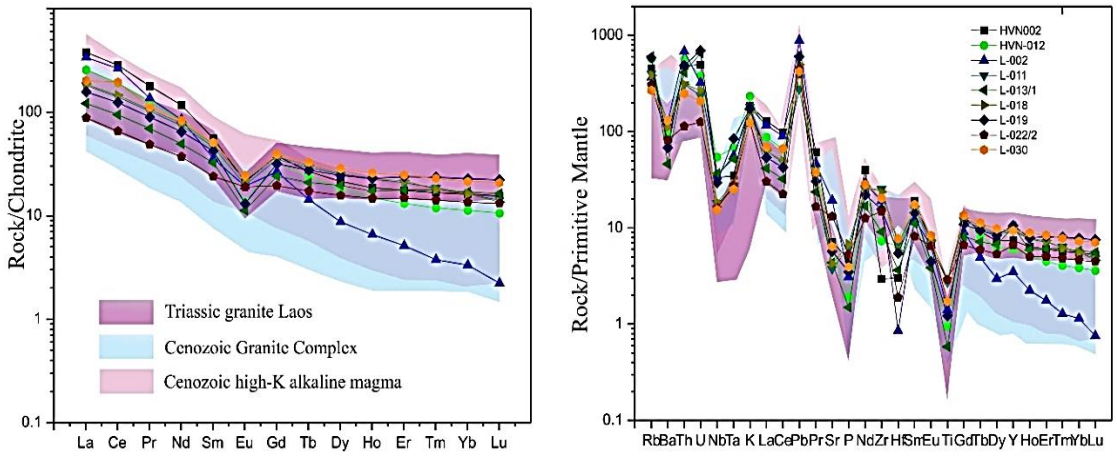

Figure 6. Trace elements of Northern Laos-Western Vietnam granites: a) Chondrite-normalized REE patterns; b) Primitive mantle-normalized trace element. The normalizing values for chondrite and primitive mantle are from Sun and McDonough (1989). Data for the Triassic granitoids Laos are from Wang et al. (2016); Cenozoic granite complex are from Tran et al. (2016); Cenozoic high K - alkaline magma are from Tran et al. (2014)

5.3. Sr-Nd-Pb isotopes

Representative whole-rock Sr-Nd-Pb isotopic data for the granite from the NL-WV are listed in Table 3. The initial $^{87}Sr/^{86}Sr$ isotopic ratios ($^{87}Sr/^{86}Sr(t)$) and εNd(t) values are calculated for the time of magma crystallization with value t = 27 Ma. The initial $^{87}Sr/^{86}Sr$ isotopic ratios and εNd(t) show broad values from 0.708507 to 0.74539 and -5.22 to -12.66, respectively. Calculated depleted mantle model age $T_{(DM)}$ ranges from 1.02 to 2.15 Ga. The Pb isotopic ratios in the NL-WV granite samples are $^{206}Pb/^{204}Pb$ = 18.864-19.392, $^{207}Pb/^{204}Pb$ = 15.736-15.841 and $^{208}Pb/^{204}Pb$ = 39.224-40.080.

Table 3. The whole-rock Sr-Nd-Pb isotopic data for the granite from NL-WV

	HVN002	HVN012	L002	L011	L013/1	L018	L019	L022/2	L030
$^{87}Sr/^{86}Sr_{(27Ma)}$	0.713024	0.710694	0.710545	0.741167	0.709902	0.745390	0.708507	0.719801	0.721407
Sm	8.28	6.75	5.30	6.86	4.83	7.30	6.27	3.55	7.60
Nd	52.83	37.73	38.27	33.56	22.36	35.53	29.31	16.77	37.80
$^{147}Sm/^{144}Nd$	0.09672	0.11043	0.08550	0.12618	0.13347	0.12679	0.13200	0.13072	0.12406
$^{143}Nd/^{144}Nd$	0.51216	0.51229	0.51229	0.51198	0.51233	0.51198	0.51236	0.51198	0.51219
$^{143}Nd/^{144}Nd_{(27Ma)}$	0.51214	0.51227	0.51227	0.51196	0.51231	0.51196	0.51234	0.51195	0.51217
$T_{(DM)}$	1.29E+09	1.28E+09	1.02E+09	2.03E+09	1.55E+09	2.05E+09	1.48E+09	2.15E+09	1.64E+09
e_{Nd} (i=27)	-8.98	-6.58	-6.42	-12.51	-5.74	-12.63	-5.22	-12.66	-8.55
e_{Nd}	-9.33	-6.87	-6.80	-12.75	-5.96	-12.87	-5.45	-12.89	-8.80
U	10.22	7.85	6.61	4.87	13.42	5.53	14.29	2.59	4.28
Th	39.82	47.44	57.00	25.91	34.21	25.84	40.52	9.46	20.78
Pb	27.60	19.45	61.85	19.44	42.35	34.70	41.71	31.08	29.45
$^{206}Pb/^{204}Pb_i$	18.955	18.888	19.046	19.392	18.946	19.226	18.896	18.864	19.081
$^{207}Pb/^{204}Pb_i$	15.768	15.720	15.737	15.841	15.736	15.845	15.724	15.758	15.792
$^{208}Pb/^{204}Pb_i$	39.554	39.396	39.654	40.080	39.365	39.909	39.287	39.224	39.580

Analyzed at the University of the Ryukyus, Japan

6. Discussions

6.1. Genetic type

Granitic rocks have been generally divided into I-, S-, M-, and A-type granites according to their geochemical and petrographic characteristics (Chappell, 1999; Chappell and White, 1992; Chappell and White, 2001; Collins et al., 1982).

The NL-WV granites have high K_2O content (3.63 to 5.46%), low FeO_T/MgO (1.79 to 5.38) (Fig. 7) and A/CNK (1.40-1.67) ratios (Fig. 5b), falling in the high-K-calc-alkaline and shoshonite series (Fig. 5b, c). On the $(Na_2O+K_2O)/CaO$ vs. $(Zr+Nb+Ce+Y)$ (Whalen et al., 1987) and FeO_T/MgO vs. SiO_2 (Eby, 1990) discrimination diagrams, the samples are of non-fractionated I-, S-type granites (Fig. 8a, b). On the ACF diagram (Chappell and White, 1992), most samples plot in S-type granite (Fig. 8c). In addition, on the Th vs. Rb diagram (Chappell, 1999), most of the analytic data plot along with the trend of S-type granite (Fig. 8d).

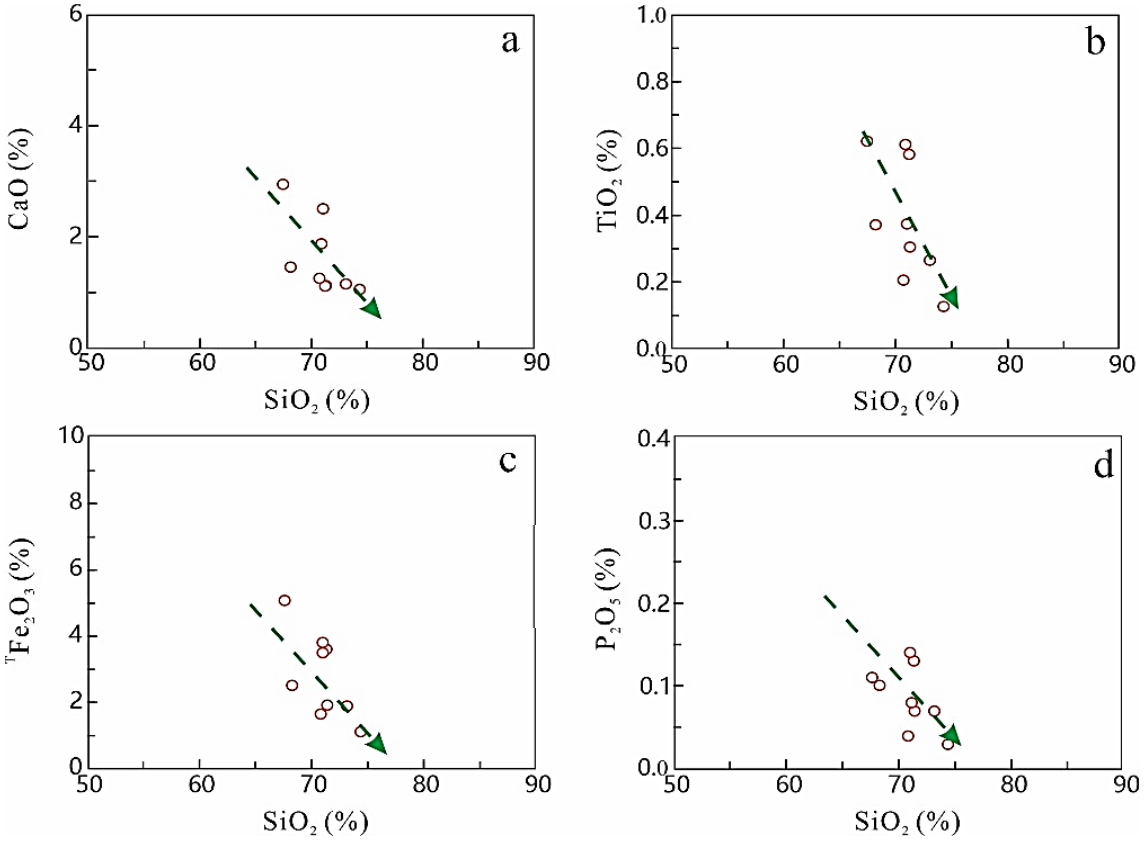

Figure 7. Harker diagram of the NL-WV granites

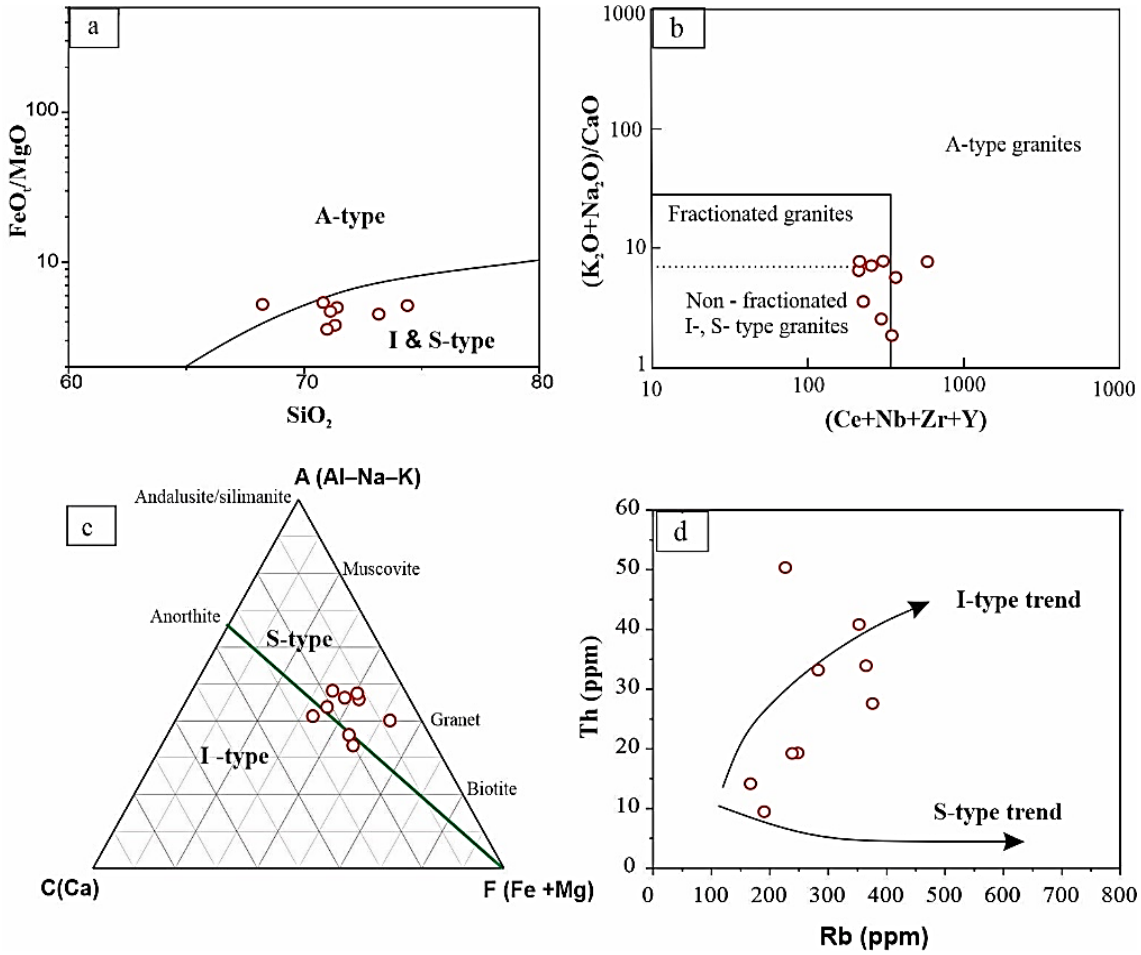

Figure 8. Granite discrimination diagrams for the NL-WV granites:
a) FeO*/MgO versus SiO_2 (Eby, 1990); b) (Na_2O+K_2O)/CaO vs. Zr+Nb+Ce+Y diagram (Whalen et al., 1987); c) ACF diagram (Chappell and White, 1992); d) Th vs. Rb (Chappell, 1999)

6.2. Source characteristics

The studies on two types of granite I and S in the Lachlan fold belt (Chappell and White, 1992, 2001) show that: S-type granite is commonly found in the thickening part of the continental plate-is the product of partial melting of sedimentary, metamorphic rocks. They carry the geochemical characteristics of sedimentary rocks quite clearly. Most of these magmatic rocks are crystallized "in-situ" from a water-saturated minimum fluid. The granitoid complex is a mixture of the minimum temperature fluid and the entity. As is known, in weathering on the surface of Na and Ca, which are often washed away from the rock, Al is enriched; at the same time, during the formation of sedimentary rocks, the K content is increased. Thus, the claystone becomes rich in Al and K (small Na/K ratio). These geochemical characteristics were shown in the granites formed from claystone by the effect of metamorphic processes (Chappell and White, 1992; Chappell, 1999). By the direct impact of temperature, the fluids become unsaturated with water, moves away from the formation site to form intrusive rocks of small size, diverged, and complete geochemical characteristics of sedimentary

origin (such as rich in potassium, supersaturated with aluminum, large Sr^{87}/Sr^{86} ratio).

On the Zr/Nd vs. Zr diagram, the NL-WV granite also shows mainly forming by the partial melting trend (Fig. 9a). Furthermore, almost all NL-WN samples have enriched LREE and depletion HREE, which is similar to the Upper continent trend (Fig. 6a) and the similar pattern between Upper continents with our sample in the spider diagram (Fig. 6b). Moreover, $^{206}Pb/^{204}Pb$ and $^{207}Pb/^{204}Pb$ ratios ranged from 18.864 to 19.392 and 15.736 to 15.841, respectively, suggesting NL-WV granites were derived from an upper continental crust (Fig. 10). The εNd(t) has a wide range (Table 3), which is similar to those of the Lachlan S-type granites (Fig. 11). It is important to note that the NL-WV maybe from by the partial melting of upper crust and mixing of the mantle- and/or sediment-derived melts to varying degrees, similar to the S-type granites from the Lachlan Fold belt in SE Australia (Chappell and White, 1992; Chappell, 1999).

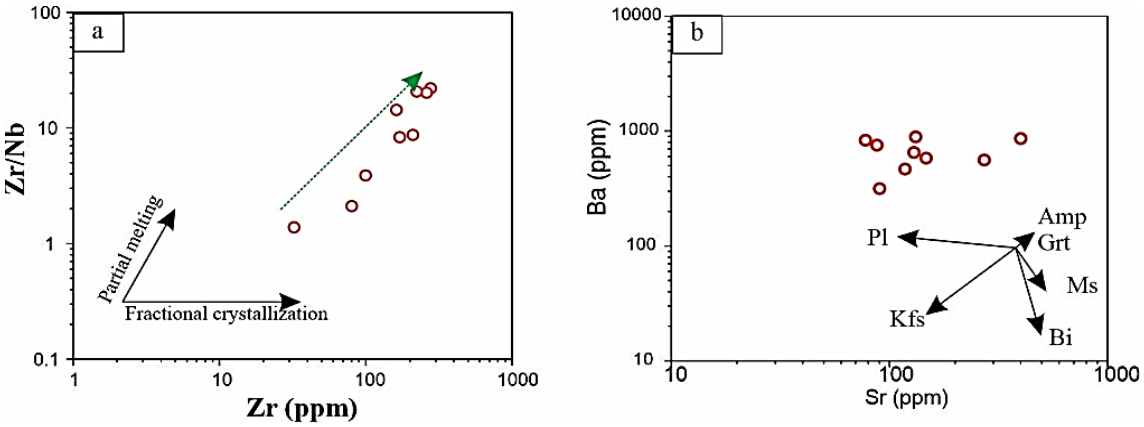

Figure 9. Trace elements ratios of NL-WV granites. a) Zr vs. Zr/Nb showing partial melting effect; b) Ba vs. Sr showing factional crystallization of plagioclase and K-feldspar

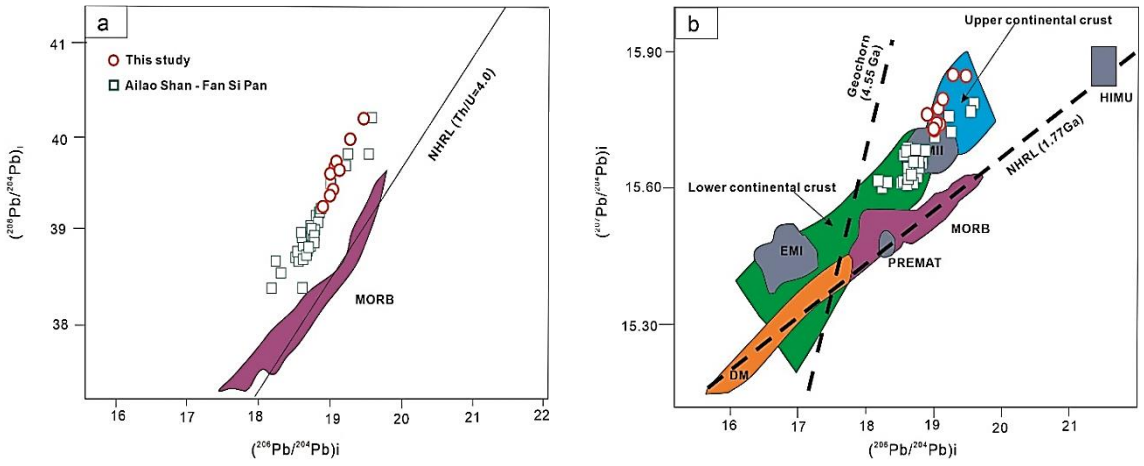

Figure 10. Pb isotopes of NL-WV granites. a) $^{208}Pb/^{204}Pb$ vs. $^{206}Pb/^{204}Pb$; b) $^{207}Pb/^{204}Pb$ vs. $^{206}Pb/^{204}Pb$ After Rollinson (1993). Ailao Shan-Fan Si Pan (Tran et al., 2014)

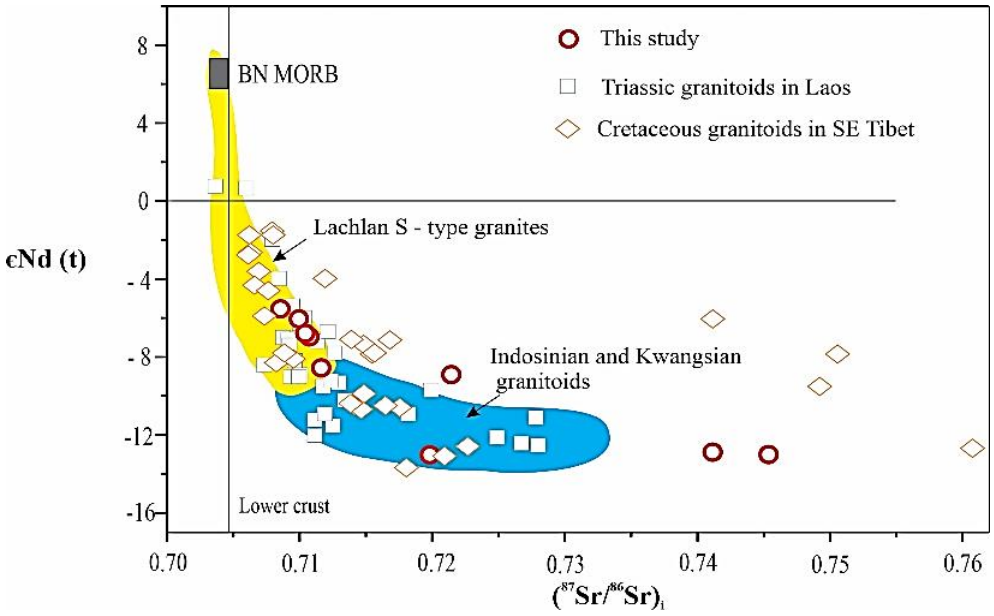

Figure 11. Whole rock εNd(t) vs. initial $^{87}Sr/^{86}$ Sr ratios of NL-WN. The BN (Bangong- Nujiang) MORB (Chen et al., 2014). Lachlan S-type granite (Healy et al., 2004). Triassic granitoids in Laos (Qian et al., 2020; Wang et al., 2016); Cretaceous granitoids in SE Tibet (Lin et al., 2012; Zhu et al., 2009)

Previous studies have shown that S-type granites can be formed by partially melting different sources (Chappell and White, 1992, 2001; Chappell, 1999). Experimental work on the metasedimentary rock suggested melting of metasedimentary, especially metagraywackes, might also generate S-type granite (Chappell, 1999). Jung and Pfänder (2007), experimentally from various materials, imply that CaO/Na_2O ratios result from partial melting of sources with different compositions (Jung and Pfander, 2007). The pelite-derived melts (CaO/Na_2O < 0.5) and melts derived from greywackes or igneous sources (CaO/Na_2O: 0.3-1.5) (Jung and Pfander, 2007). The NL-WV samples display CaO/Na_2O ratios ranger from 0.30 to 1.46, suggested their sources related to metagraywackes or igneous rock (Fig. 12a). The studied samples have variable Rb/Sr and Rb/Ba ratios, reflective of a mixed source (Douce, 1999; Patiňo-Douce, 1995; Qian et al., 2020; Sylvester, 1998) (Fig. 12b). In Fig. 12c and d, the NL-WV granites fall in the field of partial melts of metagraywackes and amphibolites. Combining the rocks' overall Sr-Nd isotope compositions, variable $^{87}Sr/^{86}Sr$ isotopic ratios of 0.708507 to 0.74539 and negative εNd(t) of -5.22 to -12.66, which also indicated these granites were produced from a mixed source of metagraywacke and mafic rock.

Most of the studied samples show an S-type geochemical affinity. On the Harker diagrams (Fig. 7), MgO, CaO, and K_2O contents decrease with SiO_2, suggesting the fractional crystallization of amphibole and plagioclase. Decreasing Fe_2O_{3t} and TiO_2 with increasing SiO_2 contents (Fig. 7c), indicate the fractional crystallization of Fe-Ti oxides minerals (e.g., ilmenite and sphene) and biotite (Pham Thi Dung et al., 2021). In addition, P_2O_5 decreases with increasing SiO_2 because apatite attains saturation in metaluminous and slightly peraluminous magmas but has a high solubility in strongly peraluminous melts (Wolf and , 1994). In the log diagrams Ba vs. Sr, fractionation of K-feldspar and plagioclase are discerned in granites from NL-WV (Fig. 9b).

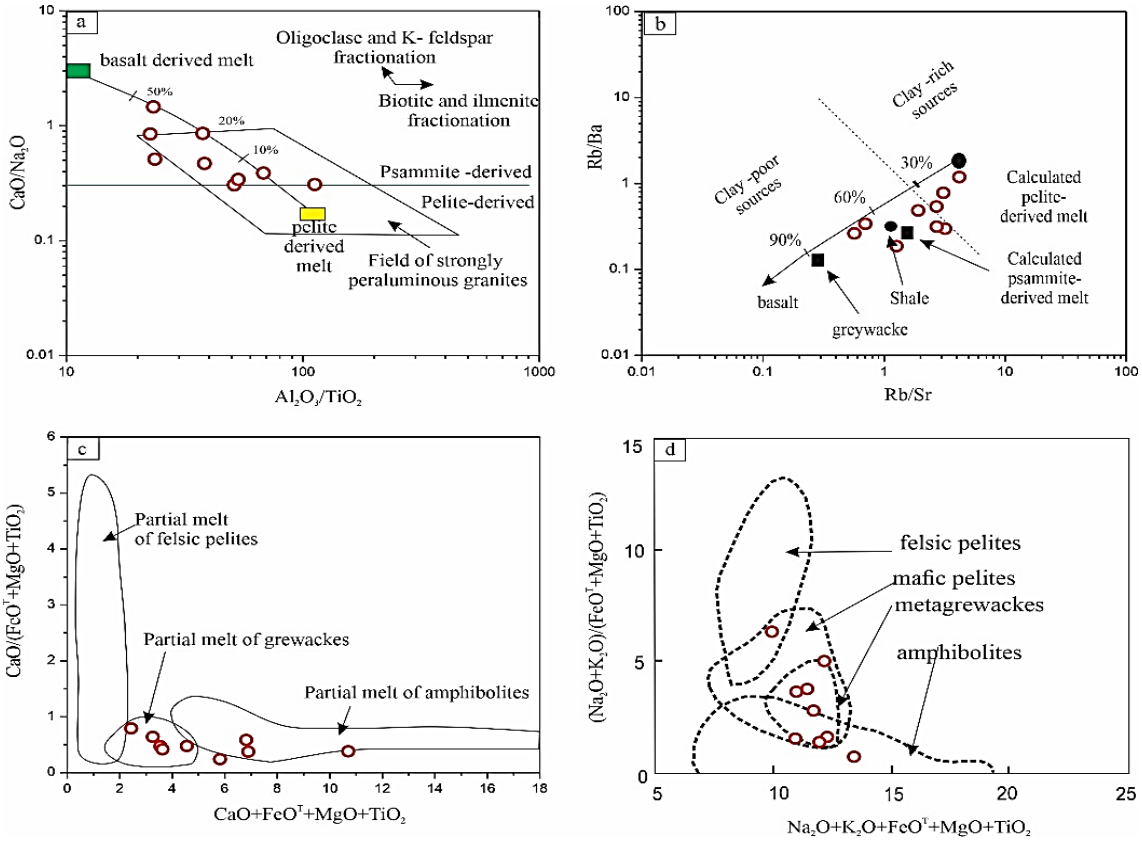

Figure 12. Source discrimination diagrams for NL-WN granites: a) CaO/Na_2O vs. Al_2O_3/TiO_2 (Sylvester, 1998); b) Rb/Ba vs. Rb/Sr after Sylvester (1998); c) and Al_2O_3 +Fe_2O_3T + MgO + TiO_2 vs Al_2O_3/(Fe_2O_3T + MgO + TiO_2) after Patiňo Douce (1999); d) Na_2O+K_2O + FeOt+MgO + TiO_2 vs (Na_2O +K_2O)/(FeOt+MgO + TiO_2) (Patiňo-Douce, 1999)

6.3. Implications for crustal evolution

Previous studies on regional tectonics have shown that the Indochina was undergone by two mainly tectonics, which is Indochina-South China subduction/collision during the Permian-Triassic (Ngo et al., 2016; Roger et al., 2012) and India-Asia collision commenced during the Cenozoic (Aitchison et al., 2007; Bui et al., 2018; Zhao et al., 2020; Hoang et al., 2016, 2017). The Cenozoic igneous activities in southeast China and Indochina occurred in two episodes at 42-24 Ma and 16-0 Ma (Fig. 13) (Wang et al., 2001). The former is related to the strike-slip faults system such as the Red River fault system that erupted synchronously with the opening of the East Vietnam Sea (EVS) (Wang et al., 2001), and the latter is coeval with east-west extension in Tibet and entire eastern Asia (Wang et al., 2001). Continental crust reconstruction the South China area at 30 to 25 Ma, the tectonic events led to EVS opening. The northward movement of Australia trapped the Indian oceanic crust in the Molucca Sea after collision in the Sulawesi and Halmahera region (Hall et al., 1997). Displacement of blocks in 30 Ma driven by the indentation of Eurasia by India (Tapponnier et al., 1982) contributed further to the closure of the proto-EVS, as Indochina was extruded SE on the Red River fault. In 25 Ma, the movement of the Indochina block on the Red River shear zone continued and

was absorbed by extension within the Sunda Shelf.

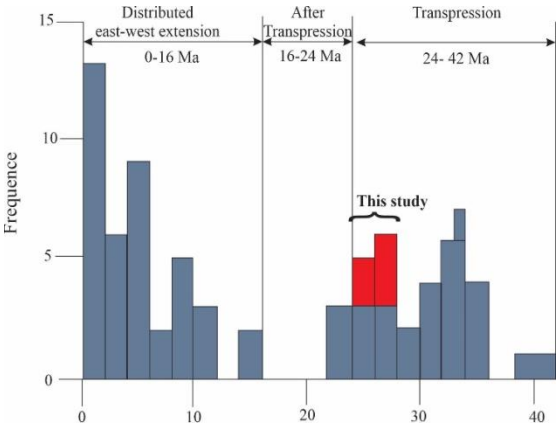

Figure 13. Statistics of tectonic activity phases in the South China-Indochina and corresponding frequency

Previous studies of tectonic-magmatic evolution in the northern Truong Son fold belt area (Jolivet et al., 1999, 2001; Lepvrier et al., 1997) showed that the Red River shear zone activity impacted during 42-24 Ma leading this area to undergo two main deformation phases. The first phase was accompanied by brittle-plastic deformation, low metamorphism related to stretching activity. This activity occurred around Late Oligocene (ca. 28-24 Ma). This process caused the continental crust to bevel and split. Magma was extruded to form a series of granite originating from the upper continental crust (Fig. 10b), the age of the formation was about 28 Ma (HVN002, HVN012, L030-2). The second deformation phase occurred in the compressive and strike-slip, brittle deformation. The second activity occurred around Early Miocene (24-20 Ma), causing the entire area to uplift, creating high temperatures to recrystallize crust components (sediment and metagraywacke metamorphism), thereby forming granite series with the ages at 24 Ma (L013-1, L019). In addition, the uplift process also causes the metamorphism of surrounding rocks, forming concentric metamorphic domes very typical in areas such as Bu Khang dome, Hanh Dich dome, Watkit dome (Laos), the core parts of metamorphic domes are granite in this study.

Our data show that the Cenozoic felsic igneous rocks in NL-WV were emplaced at 28-24 Ma, with crustal model ages are range from 1.1 Ga to 2.0 Ga. The tectonic discrimination diagrams Rb vs. Y+Nb; Rb vs. Ta+ Yb, NL-WV granite samples mainly fall into the post-collision (post-COLG) field (Pearce., 1996), suggesting their post-collision affinity (Fig. 14). Therefore, we suggest that the NL-WV intrusion was associated with transpression formed by the India-Asia collision events during Cenozoic.

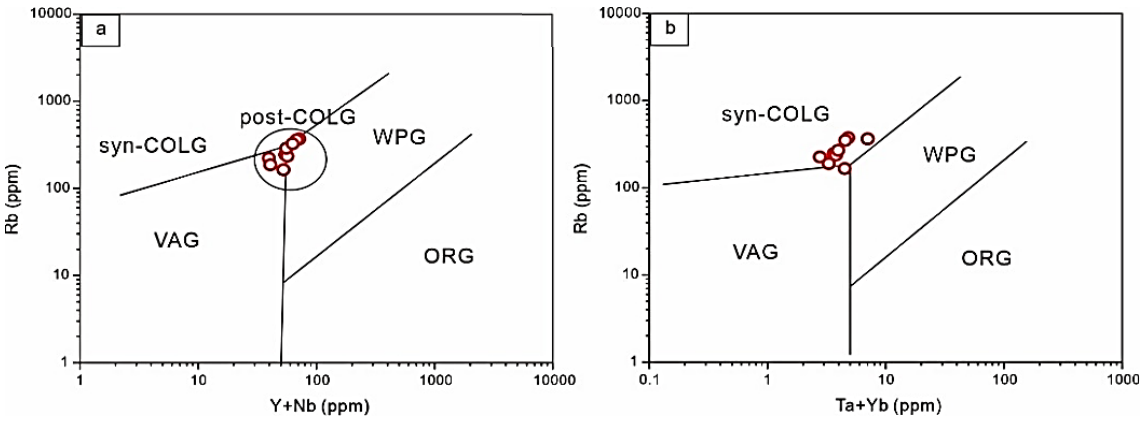

Figure 14. Tectonic discrimination diagrams of the NL-WV (Förster et al., 1997; Pearce, 1996; Pearce et al., 1984). VAG, volcanic-arc granites; WPG, within plate granites; syn-COLG, syn-collisional granites; ORG, ocean-ridge granites; post-COLG, post-collision granites

7. Conclusions

The granites from Northern Laos and Western Vietnam were formed during the Oligocene (28-24 Ma) characterized by high SiO_2, high K_2O, medium peraluminous, and S-type granite signature. The geochemical and isotopic data suggest that these granites were derived by partial melting of the Proterozoic upper crust (1.02-2.1 Ga) and mixing the mantle-and/or sediment-derived melts to varying degrees, following the India-Asia collision events during the Cenozoic.

Acknowledgements

This study is part of the Vietnam-Laos joint research project "Tectono-magmatic evolution and metallogeny of Sn, W, Au, multi-metal ore deposit in Northwestern Nghe An and Sam Nuae area" coded NĐT.35.LA/17 (Vietnam Ministry of Science and Technology) and cooperation project RFFI "Petrogenesis of the Permian-Triassic volcanic associations in the Song Hien-An Chau rift system, Northeastern Vietnam", coded QTRU01.09/20-21.

References

Aitchison J.C., Ali J.R., Davis A.M., 2007. When and where did India and Asia collide? Journal of Geophysical Research: Solid Earth, 112 (B05423). Doi: 10.1029/2006JB004706.

Bui V. Hau, Yoonsup Kim, Ngo X. Thanh, Tran T. Hai, Keewook Yi, 2018. Neoproterozoic deposition and Triassic metamorphism of metasedimentary rocks in the Nam Co Complex, Song Ma Suture Zone, NW Vietnam. Geosciences Journal, 22, 549-568.

Chappell B.W., 1999. Aluminium saturation in I- and S-type granites and the characterization of fractionated haplogranites. Lithos, 46.

Chappell B.W., White A., 1992. I-and S-type granites in the Lachlan Fold Belt. Earth and Environmental Science Transactions of the Royal Society of Edinburgh, 83(1-2), 1-26.

Chappell B.W., White A.J.R., 2001. Two contrasting granite types: 25 years later. Australian Journal of Earth Sciences, 48, 489-499.

Chen Y., Zhu D.-C., Zhao Z.-D., Meng F.-Y., Wang Q., Santosh M., Wang L.-Q., Dong G.-C., Mo X.-X., 2014. Slab breakoff triggered ca. 113Ma magmatism around Xainza area of the Lhasa Terrane. Tibet. Gondwana Research, 26(2), 449-463.

Collins W.J., Beams S.D., White A.J.R., Chappell B.W., 1982. Nature and origin of A-type granites with particular reference to Southeastern Australia. Contributions to Mineralogy and Petrology, 80(2), 189-200.

Douce A.E.P., 1999. What do experiments tell us about the relative contributions of crust and mantle to the origin of granitic magmas? Geological Society, London. Special Publications, 168(1), 55-75.

Eby G.N., 1990. The A-type granitoids; a review of their occurrence and chemical characteristics and speculations on their petrogenesis. Lithos, 26, 115-134.

Fontaine H., Workman D.R., 1978. Review of the geology and mineral resources of Kampuchea, Laos and Vietnam, 541-603. In: Nutalaya P. (Ed.), Proc. 3rd Regional Conference on Geology and Mineral Resources of Southeast Asia, 887pp.

Förster H.J., Tischendorf G., Trumbull R.B., 1997. An evaluation of the Rb vs. (Y+Nb) discrimination diagram to infer tectonic setting of silicic igneous rocks. Lithos, 40(2), 261-293.

Hall R., 1997. Cenozoic plate tectonic reconstructions of SE Asia. Geological Society of London. Special Publication, 126, 11-23.

Hamilton W., 1979. Tectonics of the Indonesian region. US Geological Survey Professional Paper, 1078, 345pp.

Healy B., Collins W., Richards S.W., 2004. A hybrid origin for Lachlan S-type granites: The Murrumbidgee Batholith example. Lithos, 78, 197-216.

Hisatoshi I., Shimpei U., Futoshi N., Shojiro N., 2017. Zircon U-Pb dating using LA-ICP-MS: Quaternary tephras in Yakushima Island, Japan. Journal of Vocanology and Geothermal Research, 338, 92-100.

Hoang N., Uto K., 2006. Upper mantle isotopic components beneath the Ryukyu arc system: Evidence for "back-arc" entrapment of Pacific MORB mantle. Earth and Planetary Science Letter, 249, 229-240.

Hoang Bac Bui, Xuan Thanh Ngo, The Hung Khuong, Jan Golonka, Tien Dung Nguyen, Yungoo Song, Tetsumaru Itaya, Koshi Yagi, 2017. Episodes of brittle deformation within the Dien Bien Phu Fault zone, Vietnam: Evidence from K-Ar age dating of authigenic illite. Tectonophysics, 695, 53-63.

Hoang Bac Bui, Xuan Thanh Ngo, Yungoo Song, Tetsumaru Itaya, Koshi Yagi, The Hung Khuong, Tien Dung Nguyen, 2016. K-Ar Dating of Fault Gouges from the Red River Fault Zone of Vietnam. Journal of the Geological Society of China, 90(5), 1653-1663.

Hoskin P.W.O., Black L.P., 2000. Metamorphic zircon formation by solid-state ecrystallization of protolith igneous zircon. Journal Metamorphic Geology, 18, 423-439.

Hutchinson R.W., 1993. A multi-stage, multi-process genetic hypothesis for greenstonehosted gold lodes: Ore Geology Reviews, 8, 349-382.

Jung S., Pfander J.r.A., 2007. Source composition and melting temperatures of orogenic granitoids: constraints from CaO/Na_2O, Al_2O_3/TiO_2 and accessory mineral saturation thermometry. European Journal of Mineralogy, 19(6), 859-870.

Jolivet L., Maluski H., Beyssac O., Goffé B., Thi P.T., Vuong N.V., 1999. Oligocene-Miocene Bu Khang extensional gneiss dome in Vietnam: Geodynamic implications. Journal of Geology, 27, 67-70.

Jolivet L., Bayssac O. Goffé B., Avigad D., Lepvrier C., Maluski H., Thang T.T., 2001. Oligo-Miocene midcrustal subhorizontal shear zone in Indochina. Journal of Tectonics, 20, 46-57.

Katili A., 1975. Volcanism and plate tectonics in the Indonesian island arcs. Tectonophysics, 26, 165-188.

Kenzo S., Hiroyasu M., Sixomxeun D., Siphandone V., Robert A.D., Yasushi W., 2011. $^{40}Ar/^{39}Ar$ ages of granitoids from the Truong Son fold belt and Kontum massif in Laos. Journal of Mineralogical and Petrological Sciences, 106, 13-25.

Lan C.Y., Chung S.L., San Shen J.J., Lo C.H., Wang P.L., Hoa T.T., Thanh H.H., Mertzman S.A., 2000. Geochemical and Sr-Nd isotopic characteristics of granitic rocks from Northern Vietnam. Journal of Asian Earth Sciences, 18, 267-280.

Lepvrier C., Maluski H., Vuong N.V., Roques D., Axente V., Rangin C., 1997. Indosinian NW-trending shear zone within the Truong Son belt (Vietnam). ^{40}Ar-^{39}Ar Triassic ages and Cretaceous to Cenozoic overprints. Tectonophysics, 283, 105-127.

Lin I.J., Chung S.L., Chu C.H., Lee H.Y., Gallet S., Wu G., Ji J., Zhang Y., 2012. Geochemical and Sr-Nd isotopic characteristics of Cretaceous to Paleocene granitoids and volcanic rocks, SE Tibet: Petrogenesis and tectonic implications. Journal of Asian Earth Sciences, 53, 131-150.

Ludwig K.R., 2003. User's Manual for Isoplot 3.0: A Geochronological Toolkit for Microsoft Excel. Berkeley Geochronology Center. Special Publication, 4, 1-71.

Maniar P.D., Piccoli P.M., 1989. Tectonic discrimination of granitoids. Geological Society of America Bulletin, 101, 635-643.

Mao H.J., 2012. Geology and Metallogeny of the Pha Lek Deposit in Truong Son belt, Laos: [Dissertation]. Chengdu University of Technology, Chengdu, 1-104.

Middlemost E.A.K., 1994. Naming Materials in the magma/igneous rock system. Earth Science Reviews, 37, 215-224.

Ngo Xuan Thanh, Tran Thanh Hai, Nguyen Hoang, Vu Quang Lan, Sanghoon Kwon, Tetsumaru Itaya, M. Santosh, 2014. Backarc mafic-ultramafic magmatism in Northeastern Vietnam and its regional tectonic significance. Journal of Asian Earth Sciences, 90, 45-60

Ngo T.X., Santosh M., Tran H.T., Pham H.T., 2016. Subduction initiation of Indochina and South China blocks: insight from the forearc ophiolitic peridotites of the Song Ma Suture Zone in Vietnam. Geological Journal, 51(3), 421-442.

Patiño-Douce A.E., Beard J.S., 1995. Dehydration-melting of biotite gneiss and quartz amphibolite from 3 to 15 kbar. Journal of Petrology, 36(3), 707-738.

Pearce J., 1996. Sources and settings of granitic rocks. Episodes, 19, 120-125.

Pearce J.A., Harris N.B.W., Tindle A.G., 1984. Trace Element Discrimination Diagrams for the Tectonic Interpretation of Granitic Rocks. Journal of Petrology, 25(4), 956-983.

Pham Thi Dung, Tran Tuan Anh, Tran Quoc Hung, Tran Trong Hoa, R.A. Shelepaev, Nguyen Hoang, Tran Quoc Cong, 2021. Petrographic and geochemical characteristics of the Nui Chua pegmatoid mafic-ultramafic series, Northern Vietnam: Significance in petrogenesis and Fe-Ti-V metallogenesis. Vietnam J. Earth Sciences, 43(1), 81-95.

Pham Ngoc Can, Tran Tuan Anh, Tran Trong Hoa, Vu Hoang Ly, Pham Thi Phuong Lien, Ngo Thi Huong, 2020. Chemical compositions of amphiboles and their references to formation conditions of granitoids from Nam Rom and Song Ma massifs, Northwest Vietnam. Vietnam J. Earth Sciences, 42(1), 80-92.

Pham Trung Hieu, Shuang-Qing Li, Yang Yu, Ngo Xuan Thanh, Le Tien Dung, Vu Le Tu, Wolfgang Siebel, Fukun Chen, 2017. Stages of late Paleozoic to early Mesozoic magmatism in the Song Ma belt, NW Vietnam: evidence from zircon U-Pb geochronology and Hf isotope composition. International Journal of Earth Sciences, 106, 855-874.

Qian X., Wang Y., Zhang Y., Wang Y., Senebouttalath V., 2020. Late Triassic post-collisional granites related to Paleotethyan evolution in Northwestern Lao PDR: Geochronological and geochemical evidence. Gondwana Research, 84, 163-176.

Rickwood P.C., 1989. Boundary lines within Petrologic diagrams which use oxides of major and minor elements. Lithos, 22, 247-263.

Roger F., Maluski H., Lepvrier C., Vu Van T., Paquette J.-L., 2012. LA-ICPMS zircons U/Pb dating of Permo-Triassic and Cretaceous magmatisms in Northern Vietnam - Geodynamical implications. Journal of Asian Earth Sciences, 48, 72-82.

Rollinson H., 1993. Using Geochemical Data: Evaluation, Presentation, Interpretation. Longman. Essex, pp.325.

Schärer U., Tapponnier P., Lacassin R., Leloup P.H., Dalai Z., Shaocheng J., 1990. Intraplate tectonics in Asia: A precise age for large-scale Miocene movement along the Ailao Shan-Red River shear zone, China. Earth and Planetary Science Letters, 97, 65-77.

Sun S.S., McDonough W.F., 1989. Chemical and isotopic systematics of oceanic basalts: Implications for mantle composition and processes. Chemical and Isotopic Systematics of Oceanic Basalts: Implications for Mantle Composition and Processes, 313-345.

Sylvester P.J., 1998. Post-collisional strongly peraluminous granites. Lithos, 45, 29-44.

Tapponnier P., Peltzer G., Le Dain A.Y., Armijo R., Cobbold P., 1982. Propagating extrusion tectonics in Area: New insights from simple experiments with plasticine. Geology, 10, 611-616.

Tran H.T., Polyakov G.V., Tran A.T., Borisenko A.S., Izokh A.E., Balykin P.A., Ngo P.T., Pham D.T., 2016. Intraplate magmatism and metallogeny of North Vietnam. Springer, 359-372.

Tran M.D., Liu J., Nguyen Q.L., Chen Y., Tang Y., Song Z., Zhang Z., Zhao Z., 2014. Cenozoic high-K alkaline magmatism and associated Cu-Mo-Au mineralization in the Jinping-Fan Si Pan region, southeastern Ailao Shan-Red River shear zone, southwestern China-northwestern Vietnam. Journal of Asian Earth Sciences, 79, 858-872.

Tran V.T., Vu K., 2011. Geology and Earth resources of Vietnam. Publising House for Science and Technology, 203-302.

Wang G.-C., Jiang Y.-H., Liu Z., Ni C.-Y., Qing L., Zhang Q., Zhu S.-Q., 2016. Multiple origins for the Middle Jurassic to Early Cretaceous high-K calc-alkaline I-type granites in northwestern Fujian province, SE China and tectonic implications. Lithos, 246-247, 197-211.

Wang J.-H., Yin A., Harrison T.M., Grove M., Zhang Y.-Q., Xie G.-H., 2001. A tectonic model for Cenozoic igneous activities in the eastern Indo-Asian collision zone. Earth and Planetary Science Letters, 188(1), 123-133.

Watson E.B., Harrison T.M., 1983. Zircon saturation revisited: temperature and composition effects in a variety of crustal magma types. Earth and Planetary Science Letters, 64, 295-304.

Wiedenbeck M., Alle P., Corfu F., Griffin W.L., Meier M., Oberli F., Quadt A.V., Roddick J.C., Spiegel W., 1995. Three natural zircon standards for U-Th-Pb, Lu-Hf, trace element and REE analyses. Geostandards and Geoanalytical Research, 19, 1-23.

Whalen J.B., Currie K.L., Chappell B.W., 1987. A-type granites: geochemical characteristics, discrimination and petrogenesis. Contributions to Mineralogy and Petrology, 95, 407-419.

Wolf M.B., London D., 1994. Apatite Dissolution into Peraluminous haplogranitic melts: An experimental study of Solubilities and 580 mechanisms. Geochimica et Cosmochimica Acta, 58(19), 4127-4145.

Zaw K., Meffre S., Lai C.K., Burrett C., Santosh M., Graham I., Manaka T., Salam A., Kamvong T., Cromie P., 2014. Tectonics and metallogeny of mainland Southeast Asia: A review and contribution. Gondwana Research, 26, 5-30.

Zhao S.-W., Lai S.-C., Pei X.-Z., Li Z.-C., Li R.-B., Qin J.-F., Zhu R.-Z., Chen Y.-X., Wang M., Pei L., 2020. Neo-Tethyan evolution in southeastern extension of Tibet: Constraints from Early Paleocene to Early Eocene granitic rocks with associated enclaves in Tengchong Block. Lithos, 105551.

Zhu D.C., Mo X.X., Wang L.Q., Zhao Z.D., Niu Y., Zhou C.Y., Yang Y.H., 2009. Petrogenesis of highly fractionated S-type granites in the Zayu area of Eastern Gangdese, Tibet: Constraints from zircon U-Pb geochronology, geochemistry and Sr-Nd-Hf isotopes. Science in China Series: Earth Sciences, 52, 1123-1239.